

Theory of intrinsic propagation losses in topological edge states of planar photonic crystals

Erik Sauer,^{1,*} Juan Pablo Vasco,^{1,2,†} and Stephen Hughes^{1,‡}

¹*Department of Physics, Engineering Physics and Astronomy,
Queen's University, Kingston, Ontario, Canada, K7L 3N6*

²*Institute of Theoretical Physics, École Polytechnique Fédérale de Lausanne EPFL, CH-1015 Lausanne, Switzerland*
(Dated: December 22, 2024)

Using a semi-analytic guided-mode expansion technique, we present the theory and analysis of intrinsic propagation losses for three topological photonic crystal slab waveguide structures with honeycomb lattices of circular or triangular holes. Although conventional photonic crystal waveguide structures, such as the W1 waveguide, have been designed to have lossless propagation modes, they are prone to disorder-induced backscattering. Topological structures have been proposed to help mitigate this effect as their photonic edge states may allow for topological protection of backscattering. However, the intrinsic propagation losses of these structures are not well understood and the concept of the light line becomes blurred. Traditional numerical methods, such as the finite-difference time-domain method, are not very efficient for computing such losses. Therefore, the semi-analytical guided-mode expansion method is a natural method of choice to analyze these structures. For the three example topological edge-state structures, photonic band diagrams, loss parameters, and electromagnetic fields of the guided modes are computed. Results show that these topological structures have significant intrinsic propagation losses, more than 100 dB/cm, which is comparable to or larger than typical disorder-induced losses using slow-light modes in conventional photonic crystal waveguides.

I. INTRODUCTION

Semiconductor photonic crystals (PCs) are dielectric structures that allow the manipulation of light on the nanoscale. Such manipulation of light can be achieved by tailoring the periodicity of the dielectric constant¹⁻⁴. In particular, planar photonic crystal slabs (PCSs) have a two-dimensional in-plane periodicity in their lattice structure, which can be used to realize slow light modes on semiconductor chips⁵. These PCSs are also often introduced with defects within their lattice structures to create waveguides^{3,6-12}, which allow the propagation of light in a particular direction, or cavities¹³⁻²⁴, thus allowing the confinement of light. The fabrication of these types of structures is usually done through semiconductor growth techniques², such as etching²⁵ or lithography²⁶.

The PCSs combine the features of two-dimensional photonic crystals, which control the in-plane propagation of light with Bragg reflection, and slab waveguides, which control the vertical propagation of light with total internal reflection. Slabs are generally used when the confinement of light in the vertical direction is desired²⁷. By combining slabs with two-dimensional waveguides, light is able to be manipulated both in-plane and vertically. Light modes leaking out from the slab lie above the light line and are “quasiguidded modes” that are subject to intrinsic losses²⁸.

Conventional PCS waveguide structures, such as the W1 waveguide (i.e., a single row of missing holes), have been studied extensively^{2,29}. For example, Kuramochi *et al.*³⁰ have achieved losses as low as 5 dB/cm, and O’Faolain *et al.*³¹ as low as 15 dB/cm. Variations of the W1 design can help improve these numbers somewhat in terms of reducing the loss per group index^{32,33}. How-

ever, in all of these conventional designs, operation near the mode edge becomes impractical because of significant disorder-induced backscattering^{2,29,34-42}.

It has been recently proposed that topological structures can help mitigate the problem of disorder-induced losses, thanks to the special properties of their photonic edge states. These edge states of topological waveguides may allow scatter-free propagation for nanoscale PCs and are known to have applications in quantum computing due to their strong interactions with quantum emitters⁴³⁻⁵⁰. Electromagnetic modes for these topological edge states have been experimentally measured by Barik *et al.*⁵¹, indicating that these topological edge states can function as waveguides, which local spin control. However, for a PCS geometry, the role of out-of-plane losses on the propagating modes is not well understood as the concept of the light line might be ill-defined for these mixed lattice structures. Therefore, quantifying such radiative losses is fundamental to fully characterize the topological edge states in PCSs.

To properly understand the behaviour of light within PCSs, solving Maxwell’s equations in the full three-dimensional geometry is required. Well-known numerical approaches, such as the finite-difference time-domain (FDTD) method⁵² or the plane wave expansion (PWE) method^{53,54}, have been commonly employed during the last two decades. The need for using numerical methods is because Maxwell’s equations cannot be solved analytically for complex structures⁵⁵⁻⁵⁸. For example, using FDTD techniques directly solves Maxwell’s equations by iterating through time. Its solutions are numerically exact, however it is a brute-force method which can be computationally inefficient^{55,59}. This computational inefficiency is especially clear when computing modes above

the light line in 3D, as the computational space becomes quite large, thus significantly increasing the runtime, and lossy modes can be hard to resolve with a time-dependent solution. The PWE method, on the other hand, works in the frequency domain rather than in the time domain. This numerical method solves Maxwell's equations as an eigenvalue problem and is significantly more efficient than FDTD. However, a major limitation with PWE is that it assumes periodicity in all spatial directions. As a result, PWE can only be accurately used for lossless systems and modes, such as standard PCs below the light line. This limitation becomes evident for PCSs, since the PWE does not (and cannot) include leaky modes in the basis expansion and therefore out-of-plane losses cannot be directly estimated^{2,27}.

An alternative method to the brute-force solvers is the semi-analytical method originally proposed by Andreani and Gerace known as the guided-mode expansion (GME)²⁸ method. In the GME, the magnetic field of the PCS is expanded in the basis of the guided mode of the slab's effective waveguide, and the resulting eigenvalue equation is solved numerically. The benefits of the GME method are two-fold: (i) it is much more computationally efficient than other numerical methods such as FDTD, because the matrix elements of the Maxwell operator become analytical in the guided mode basis; and (ii) the imaginary part of the eigenvalue, which accounts for the out-of-plane losses, can be easily estimated by means of time-dependent perturbation theory in the low loss regime. This makes GME an ideal theoretical tool for solving PCSs when the imaginary part of the mode frequency is much smaller than its real part. The GME method is therefore an excellent method of choice to analyze the intrinsic propagation losses in the edge states of topological PCS structures above the light line.

In this paper, we apply the GME method to study three different topological PCS structures, which are taken after recent designs and experiments in the literature: two separate structures proposed by Anderson and Subramania⁴³, and one proposed by Barik *et al.*⁴⁴. Anderson and Subramania earlier presented two topological structures for a modified honeycomb lattice of circular holes, each with a different interface between the topological and trivial lattices: one with an armchair interface and one with a zigzag interface. Anderson and Subramania show theoretical photonic band structure calculations, as well as power flow diagrams along the interfaces. However, losses were not considered for these two structures. Barik *et al.* introduced a similar topological structure with a modified honeycomb lattice⁴⁴, but with triangular holes separated by an armchair interface. The interactions between this structure and quantum emitters have been investigated experimentally, and electromagnetic modes have been found⁵¹. Some partial loss calculations for this structure are available in the supplementary material of Ref. 51, which are presented in the form of minimum propagation length using brute-force numerical solutions. Experimentally, a loss length of 22

μm has been shown for this structure, and they have predicted that a loss length of up to 40 μm can be achieved with appropriate parameter adjustments. With such a brute-force FDTD approach, the origin of such losses is not so clear; alternative techniques are needed not only to highlight the underlying physics, but also to explore parameter space for lower loss designs.

II. TOPOLOGICAL PHOTONIC CRYSTAL STRUCTURES OF INTEREST

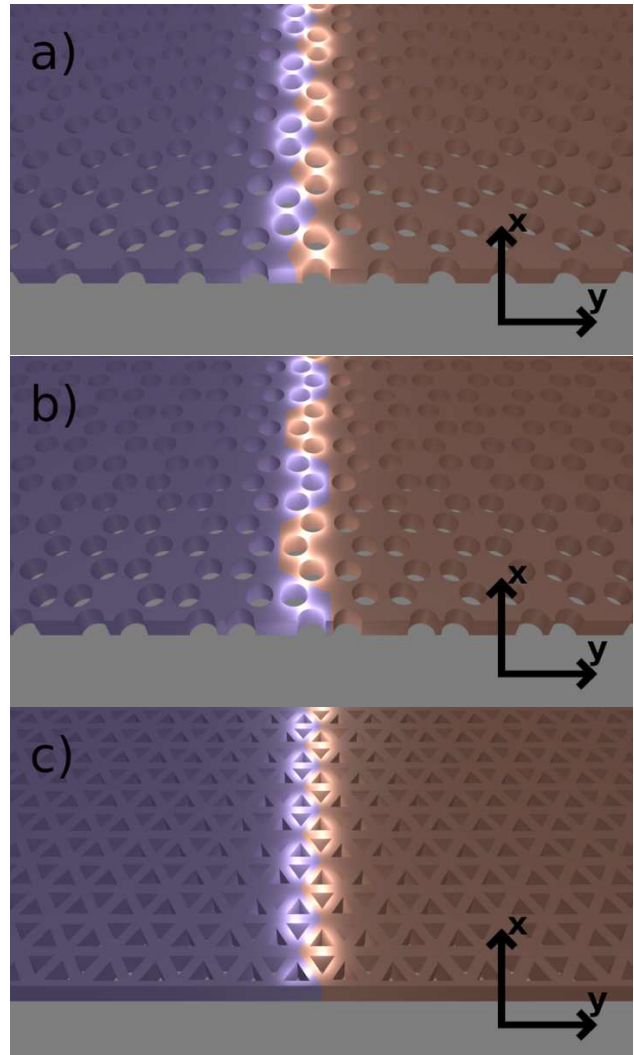


Figure 1. Schematic 3D models of the PCS structures of interest that are studied in this work, with: (a) an armchair interface, (b) a zigzag interface, and (c) a triangular hole armchair interface. The interfaces for these structures separate a topologically trivial lattice structure with shrunken honeycomb clusters (blue, left) and a topologically non-trivial lattice structure with expanded honeycomb clusters (brown, right).

Figure 1 shows 3D models of the three structures

studied in this work. For all three models, the interface separates a topologically trivial lattice structure with shrunken honeycomb clusters and a topologically non-trivial lattice structure with expanded honeycomb clusters. These structures will be analyzed using the GME approach in order to compute the radiative losses above the light line. Our goal is to identify the regions where out-of-plane losses are minimized and characterize the corresponding intensity profiles of these quasi-guided modes. All structural parameters used from now on are taken from Refs. 43 and 44.

III. THEORY

For linear and non-magnetic media, one can rewrite Maxwell's equations in the frequency domain, such that a second-order eigenvalue equation in terms of the magnetic field $\mathbf{H}(\mathbf{r})$ is obtained:

$$\nabla \times \left[\frac{1}{\epsilon(\mathbf{r})} \nabla \times \mathbf{H}(\mathbf{r}) \right] = \left(\frac{\omega}{c} \right)^2 \mathbf{H}(\mathbf{r}), \quad (1)$$

where $\epsilon(\mathbf{r})$ is the dielectric constant of the slab. To solve this eigenvalue problem using the GME method, the magnetic field is expanded in an orthonormal set of basis states:

$$\mathbf{H}(\mathbf{r}) = \sum_{\mu} c_{\mu} \mathbf{H}_{\mu}(\mathbf{r}), \quad (2)$$

with the orthonormality condition,

$$\int_{\text{unit cell}} d\mathbf{r} \mathbf{H}_{\mu}^*(\mathbf{r}) \cdot \mathbf{H}_{\nu}(\mathbf{r}) = \delta_{\mu,\nu}. \quad (3)$$

Then, Eq. (1) is rewritten as a linear eigenvalue problem:

$$\sum_{\nu} \mathcal{H}_{\mu\nu} c_{\nu} = \frac{\omega^2}{c^2} c_{\mu}, \quad (4)$$

where the matrix elements $\mathcal{H}_{\mu\nu}$ are defined as

$$\mathcal{H}_{\mu\nu} = \int \frac{1}{\epsilon(\mathbf{r})} (\nabla \times \mathbf{H}_{\mu}^*(\mathbf{r})) \cdot (\nabla \times \mathbf{H}_{\nu}(\mathbf{r})) d\mathbf{r}. \quad (5)$$

To solve for $\mathcal{H}_{\mu\nu}$, the GME method involves solving for the magnetic field for each Bloch wave vector \mathbf{k} as a sum of the guided modes over the reciprocal lattice vectors and the mode index α . Therefore, the GME for the magnetic field can be rewritten as

$$\mathbf{H}_{\mathbf{k}}(\mathbf{r}) = \sum_{\mathbf{G}, \alpha} c(\mathbf{k} + \mathbf{G}, \alpha) \mathbf{H}_{\mathbf{k}+\mathbf{G}, \alpha}^{\text{guided}}(\mathbf{r}), \quad (6)$$

where \mathbf{G} is a reciprocal lattice vector for the PCS's lattice structure. The analytical definition for the guided mode $\mathbf{H}_{\mathbf{k}+\mathbf{G}, \alpha}^{\text{guided}}(\mathbf{r})$ varies depending on the slab's layer, and whether the mode is transverse electric (TE) or transverse magnetic (TM)²⁸. Notice that the matrix elements

$\mathcal{H}_{\mu\nu}$ in Eq. (4) depend on the Fourier transform of the inverse dielectric function in each slab layer $j = \{1, 2, 3\}$, through

$$\eta_j(\mathbf{G}, \mathbf{G}') = \frac{1}{A} \int_{\text{cell}} \epsilon_j(\boldsymbol{\rho})^{-1} e^{i(\mathbf{G}' - \mathbf{G}) \cdot \boldsymbol{\rho}} d\boldsymbol{\rho}, \quad (7)$$

where $\boldsymbol{\rho} = (x, y)$. However, from a numerical perspective, it is much more convenient to calculate the matrix elements of the dielectric function directly as²⁸

$$\epsilon_j(\mathbf{G}, \mathbf{G}') = \frac{1}{A} \int_{\text{cell}} \epsilon_j(\boldsymbol{\rho}) e^{i(\mathbf{G}' - \mathbf{G}) \cdot \boldsymbol{\rho}} d\boldsymbol{\rho}, \quad (8)$$

and use numerical matrix inversion to find $\eta_j(\mathbf{G}, \mathbf{G}') = \epsilon_j^{-1}(\mathbf{G}, \mathbf{G}')$. This is the approach that we take.

The guided mode basis is computed in an effective homogeneous slab whose dielectric constant is usually taken as the spatial average of $\epsilon_j(\boldsymbol{\rho})$:

$$\bar{\epsilon}_j = 1/A \int_{\text{cell}} \epsilon_j(\boldsymbol{\rho}) d\boldsymbol{\rho}, \quad (9)$$

where A is the unit cell area and j represents one of the slab's three layers: the lower cladding, the core and the upper cladding. Once the magnetic field is obtained from Eq. (6), the electric field is obtained by

$$\mathbf{E}_{\mathbf{k}}(\mathbf{r}) = \frac{ic}{\omega \epsilon(\mathbf{r})} \times \mathbf{H}_{\mathbf{k}}(\mathbf{r}), \quad (10)$$

where

$$\int_{\text{unit cell}} d\mathbf{r} \epsilon(\mathbf{r}) \mathbf{E}_{\mathbf{k}}^*(\mathbf{r}) \cdot \mathbf{E}_{\mathbf{k}'}(\mathbf{r}) = \delta_{\mathbf{k}, \mathbf{k}'}. \quad (11)$$

Although performing the GME in this way is accurate for photonic modes below the light line, it does not take possible out-of-plane losses into account. However, since such losses are small, one can estimate these losses perturbatively. When a photonic mode escapes the slab's core into the claddings, it couples to lossy radiation modes and falls above the light line. The mode becomes quasiguided and is now subject to intrinsic losses, which can be accurately computed from the imaginary part of the eigenfrequency, $\text{Im}(\omega)$. Similarly to the Fermi's golden rule from quantum mechanics, these losses can be computed by second-order time-dependent perturbation theory²⁸,

$$-\text{Im} \left(\frac{\omega_{\mathbf{k}}^2}{c^2} \right) = \pi \sum_{\mathbf{G}'} \sum_{\lambda} \sum_{j=1,3} |\mathcal{H}_{\mathbf{k}, \text{rad}}|^2 \rho_j \left(\mathbf{k} + \mathbf{G}'; \frac{\omega_{\mathbf{k}}^2}{c^2} \right), \quad (12)$$

where λ represents either a TE or TM mode, and the matrix element between a guided and lossy radiation mode is given by

$$\mathcal{H}_{\mathbf{k}, \text{rad}} = \int \frac{1}{\epsilon(\mathbf{r})} (\nabla \times \mathbf{H}_{\mathbf{k}}^*(\mathbf{r})) \cdot (\nabla \times \mathbf{H}_{\mathbf{k}+\mathbf{G}', \lambda, j}^{\text{rad}}(\mathbf{r})) d\mathbf{r}, \quad (13)$$

and ρ_j is the one-dimensional photonic density of states for a given wave vector $\mathbf{g} = \mathbf{k} + \mathbf{G}$ in layer j :

$$\rho_j \left(\mathbf{g}; \frac{\omega^2}{c^2} \right) = \frac{\bar{\epsilon}_j^{-1/2} c}{4\pi} \frac{\theta \left(\omega^2 - \frac{c^2 g^2}{\bar{\epsilon}_j} \right)^{-1/2}}{\left(\omega^2 - \frac{c^2 g^2}{\bar{\epsilon}_j} \right)^{-1/2}}, \quad (14)$$

with θ representing the Heaviside step function. Similarly to those for the guided modes, the analytical definitions for the radiation modes $H_{\mathbf{k}+\mathbf{G}',\lambda,j}^{\text{rad}}(\mathbf{r})$ depend on the slab's layer and polarization²⁸. Finally, the imaginary part of the frequency is obtained from:

$$\text{Im}(\omega_k) = \frac{\text{Im}(\omega_k^2)}{2\text{Re}(\omega_k)}. \quad (15)$$

IV. NUMERICAL RESULTS: COMPLEX BAND STRUCTURES AND PROPAGATION LOSSES

In this section, we apply the GME to the three topological PCS structures shown in Fig. 1. For each of the three designs, photonic band diagrams in the k_x direction are computed, along with the nominal light line. Since these band diagrams are symmetric about $k_x = 0$, only the results for $k_x \geq 0$ are shown. The topological edge states are represented by two of the bands and are shown below in a zoomed-in region of interest. Propagation losses for the two topological states within the regions of interest are also presented in terms of loss length L_α and group index $n_g = |c/v_g|$, where v_g is the group velocity. Using the fact that $\mathbf{D} = \epsilon\epsilon_0\mathbf{E}$, normalized electric displacement fields of the guided modes at the points of minimum loss for these two states are also shown, which gives a visual representation of how well the modes remain confined along the waveguides for their respective topological structure. If these modes were truly bound, then such intrinsic losses would be zero, as is usually the case for W1-like modes.

The computational implementation of the GME for the structures below was done via MATLAB. To obtain all necessary results, a choice in the number of \mathbf{k} points and the number of basis states were chosen for the dispersion calculations. These numbers are dependent on PCS structure. For the structures we analyze below, both the armchair and zigzag interface structures of circular holes use a total of 81 basis states and 1002 \mathbf{k} points. For the armchair interface structure of triangular holes, a total of 144 basis states were computed with a total of 3002 \mathbf{k} points. For all three structures, the cut-off in reciprocal lattice vectors \mathbf{G} was set to 30.

A. Armchair Interface of Circular Holes

We first show results for the PCS structure of the armchair interface of circular holes, proposed by Ander-

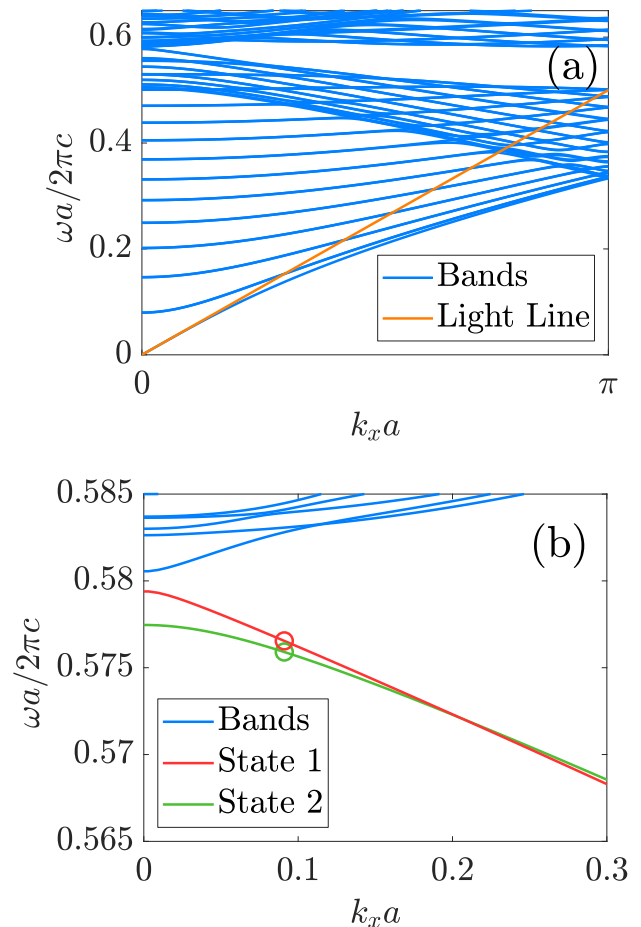


Figure 2. (a) Broadband photonic dispersion for the armchair interface structure of circular holes. (b) Zoom-in of the photonic dispersion for the armchair interface structure of circular holes, showing the upper and lower guided bands, as well as the points at which the field mode profiles are computed.

son and Subramania⁴³. The GME computations use a slab dielectric constant of $\epsilon_s = 11.5$, a slab thickness of $d = 0.25a$, a hole radius of $r = 0.13a$ and a lattice constant of $a = 870$ nm. Assuming the radius of each honeycomb cluster is R and the lattice constant is a , the topologically non-trivial side has expanded honeycomb clusters with $R_{\text{exp}} = a/2.9$ and the topologically trivial side has shrunken honeycomb clusters with $R_{\text{shr}} = a/3.1$.

Figure 2 shows the photonic band diagram for this topological structure, assuming propagation in the x direction. One might expect the topological edge states in this case to be below the light line, however the GME identifies them to be entirely above the light line due to having non-zero losses. It is important to note that the propagation losses here do not arise from backscattering, but rather from radiation leaking from the plane while the mode is propagating along the waveguide. The zoomed-in region of interest indicates the point of minimum loss at $k_x a = 0.09102$. Fig. 3 displays the propagation losses for this structure, indicating that the loss

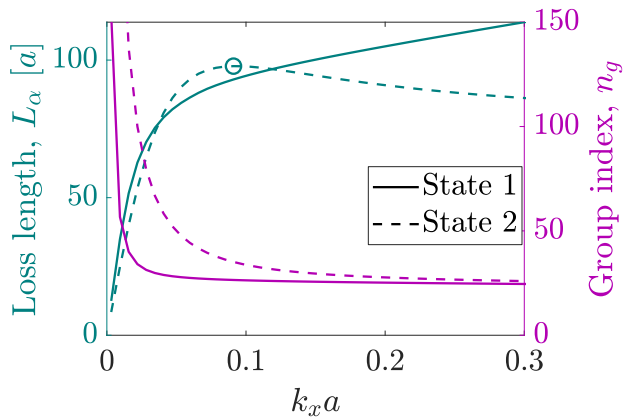


Figure 3. Loss propagation parameters for the armchair interface structure of circular holes: loss length, L_α , and the group index, $n_g = |c/v_g|$. Point of minimum loss for State 2 is indicated by a circle at $k_x a = 0.09102$, giving a loss of 510 dB/cm, assuming $a = 870$ nm⁴³.

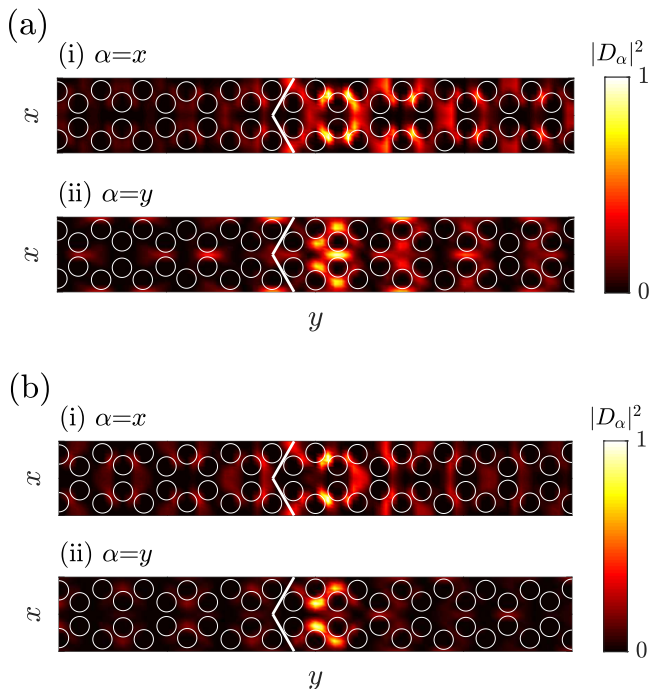


Figure 4. The x and y components of the electric displacement field profile of the guided modes for the armchair interface structure of circular holes at $z = 0$. These modes are taken at the point of minimum loss, $k_x a = 0.09102$, for (a) the upper guided band labelled as State 1 in Fig. 2 and (b) the lower guided band labelled as State 2 in Fig. 2.

length at minimum propagation loss is $L_\alpha = 97a$, and finite throughout all of \mathbf{k} space. Assuming the lattice constant of $a = 870$ nm, the minimum losses in this structure were found to be equal to 510 dB/cm, which is significantly larger than typical disorder-induced losses of conventional PC modes^{2,29-31,33,36}, which are around 5-30 dB/cm for the fast light regimes, and around 100-

1000 dB/cm for the slow light regime ($n_g \approx 100$). For thin samples, the disorder-induced losses scale inversely with the group index squared^{2,35}. The above light-line intrinsic losses of W1 waveguides have also been measured to be around 400 dB/cm³⁰, which is close to the values of the topological edge states.

The x and y components of the Bloch-mode displacement fields \mathbf{D} at $z = 0$ (i.e., in the vertical centre of the slab) are shown in Fig. 4. These modes, shown for State 1 and State 2 from Fig. 2, are taken at the points of minimum loss. As expected, the modes remain mostly along the interface, however they are still quite lossy and confinement seems to be rather poor for these edge states.

B. Zigzag Interface of Circular Holes

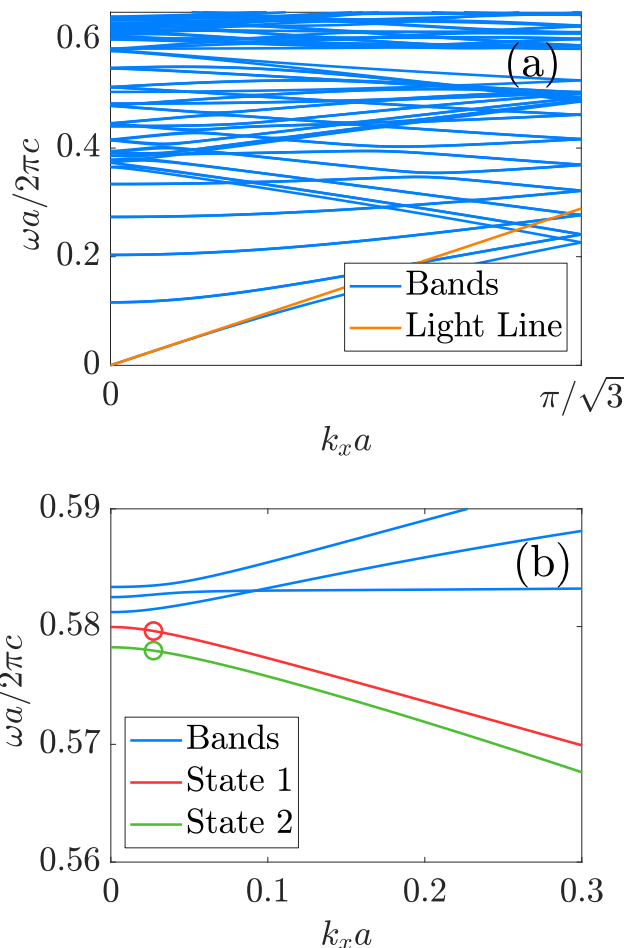


Figure 5. (a) Broadband photonic dispersion for the zigzag interface structure of circular holes. (b) Zoom-in of the photonic dispersion for the zigzag interface structure of circular holes, showing the upper and lower guided bands, as well as the points at which the field mode profiles are computed.

Next, we study the results for the PCS structure of the zigzag interface of circular holes, also proposed by Anderson and Subramania⁴³. Similar to the PCS structure of

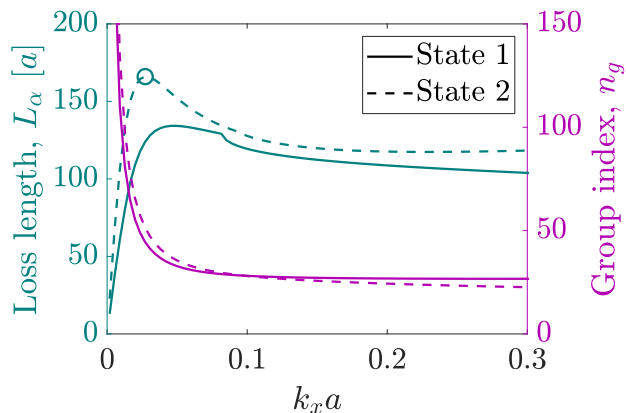


Figure 6. Loss propagation parameters for the zigzag interface structure of circular holes: loss length, L_α , and the group index, $n_g = |c/v_g|$. Point of minimum loss for State 2 is indicated by a circle at $k_x a = 0.02718$, giving a loss of 301 dB/cm, assuming $a = 870$ nm.

the armchair interface of circular holes, the GME computation used a slab dielectric constant of $\epsilon_s = 11.5$, a slab thickness of $d = 0.25a$, a hole radius of $r = 0.13a$ and a lattice constant of $a = 870$ nm. Additionally, the size of the expanded and shrunken honeycomb clusters remain consistent with the armchair interface, with $R_{\text{exp}} = a/2.9$ and $R_{\text{shr}} = a/3.1$.

The photonic band diagram and its zoom-in on the region of interest for this topological structure are shown in Fig. 5, assuming, as before, propagation in the x direction. Once again, one may naively assume that these topological edge states reside above the light line, but that is not true for the mixed lattice structure; minimum propagation losses now occur at $k_x a = 0.02718$, as indicated on Fig. 6, which yield a maximum loss length of $L_\alpha = 166a$. With a lattice constant of $a = 870$ nm, the minimum losses were found to be equal to 301 dB/cm. Although performing somewhat better than the armchair interface structure of circular holes, this PCS structure is still significantly more lossy than typical disorder-induced losses from regular PC modes.

The Bloch modes (\mathbf{D} field) for $z = 0$ are shown in Fig. 7. Despite being less lossy than the previous topological PCS structure, these modes are significantly lossy as a waveguide structure. Note also that these calculations are for the perfect structure with no structural disorder. However, the physics of these topological structures is much richer than regular PC modes^{43,44}, and these loss lengths are certainly large enough to probe many finite-size waveguide effects, exploiting topology-dependent spin⁵¹.

C. Armchair Interface of Triangular Holes

We next consider the PCS structure of the armchair interface of triangular holes initially proposed by Barik

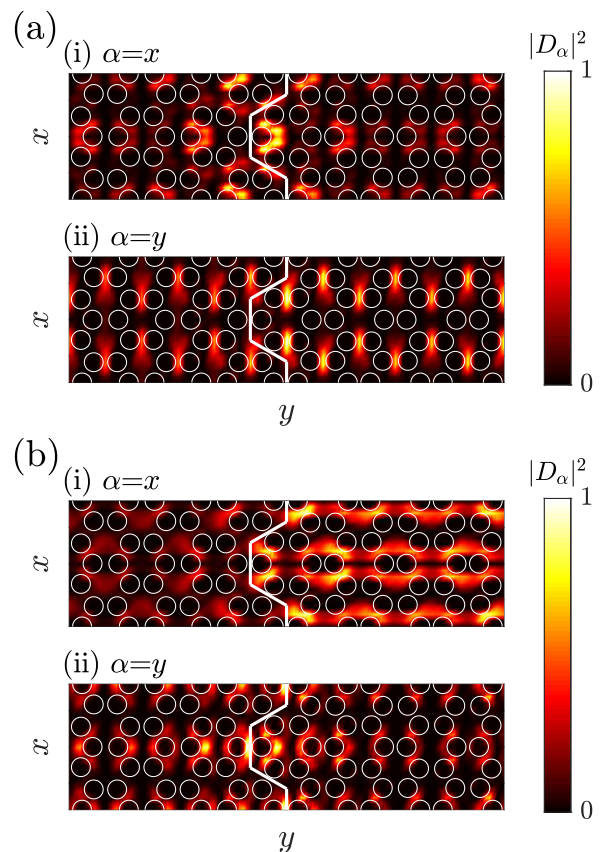


Figure 7. The x and y components of the electric displacement field profile of the guided modes for the zigzag interface structure of circular holes at $z = 0$. These modes are taken at the point of minimum loss, $k_x a = 0.02718$, for (a) the upper guided band labelled as State 1 in Fig. 5 and (b) the lower guided band labelled as State 2 in Fig. 5.

et al. in 2016⁴⁴, and later examined experimentally by coupling spin-dependent quantum dots in 2018⁵¹. The GME computation uses the following parameters: a slab dielectric constant of $\epsilon_s = 12.11$, a slab thickness of $d = 160a/445$, a length of one side of the equilateral triangular hole of $L = 140a/445$ and a lattice constant of $a = 445$ nm. In this case, the topologically non-trivial side has expanded honeycomb clusters with $R_{\text{exp}} = 1.05a/3$ and the topologically trivial side has shrunken honeycomb clusters with $R_{\text{shr}} = 0.94a/3$.

We show in Fig. 8 the photonic band diagram for this topological structure, along with its zoom-in of the region of interest. Propagation is assumed to be in the x direction once again, however the topological edge states are not fully above the light line in this case. State 1 resides above the light line for $|k_x a| < 3.0495$, whereas State 2 resides above the light line for $|k_x a| < 2.6286$. Minimum losses occur at $k_x a = 0.017796$, and the loss propagation parameters are shown in Fig. 9. The loss length achieved at the point of minimum loss is equal to $L_\alpha = 79a$, and the minimum propagation losses were found to be equal to 1242 dB/cm. This PCS structure seems to perform

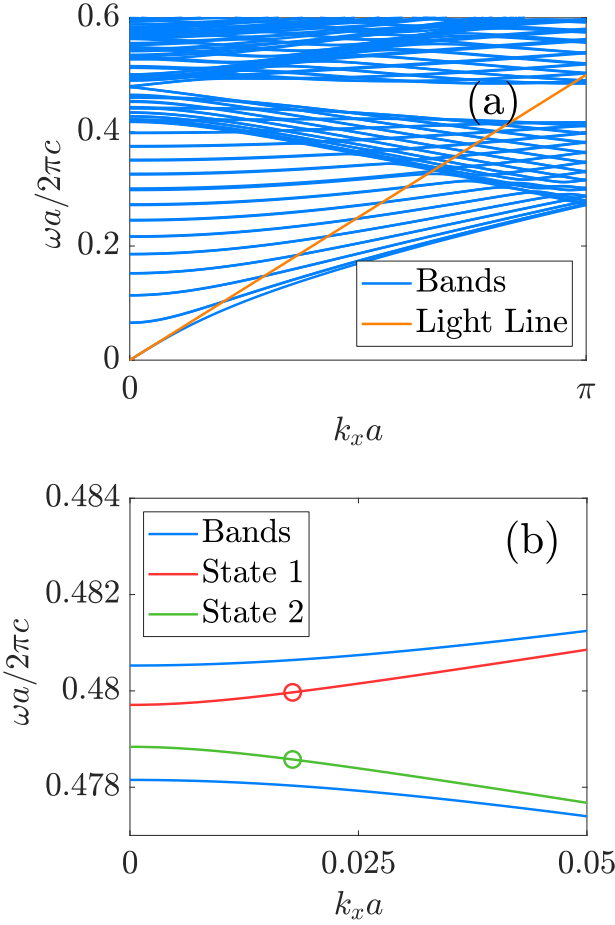


Figure 8. (a) Broadband photonic dispersion for the armchair interface structure of triangular holes. (b) Zoom-in of the photonic dispersion for the topological triangular hole structure, showing the upper and lower guided bands, as well as the points at which the field mode profiles are computed.

the worst among the three designs; it has much more significant losses on the order of 10^3 rather than 10^2 .

Barik *et al.* have performed experimental work on this structure and have acquired some values for loss length⁵¹. Knowing that a lattice constant of $a = 445$ nm was used, the loss length of $L_\alpha = 79a$ for this structure is equivalent to $L_\alpha = 35$ μm . Comparing this loss length with their experimental value of 22 μm , it is clear that these two values are within the same order of magnitude.

Figure 10 shows the components of the guided mode's electric displacement field for this structure at $z = 0$. Similarly to the two other topological structures, the modes remain mostly along the interface, however the edge state confinement is significantly worse in this case.

V. CONCLUSIONS

In this work, we have applied the guided-mode expansion method to three topological photonic crystal slab

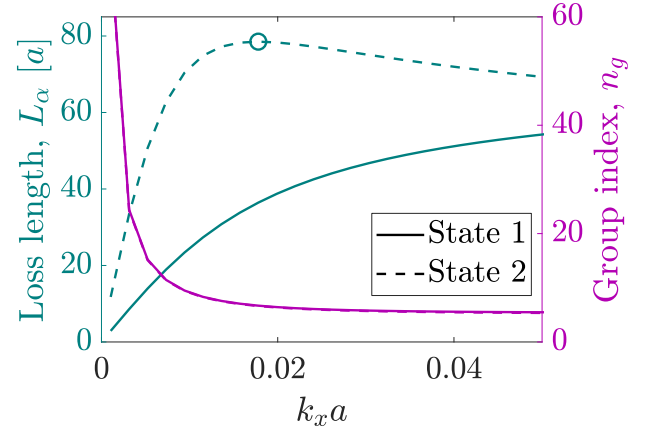


Figure 9. Loss propagation parameters for the armchair interface structure of triangular holes: loss length, L_α , and the group index, $n_g = |c/v_g|$. Point of minimum loss for State 2 is indicated by a circle at $k_x a = 0.017796$, giving a loss of 1242 dB/cm, assuming $a = 445$ nm.

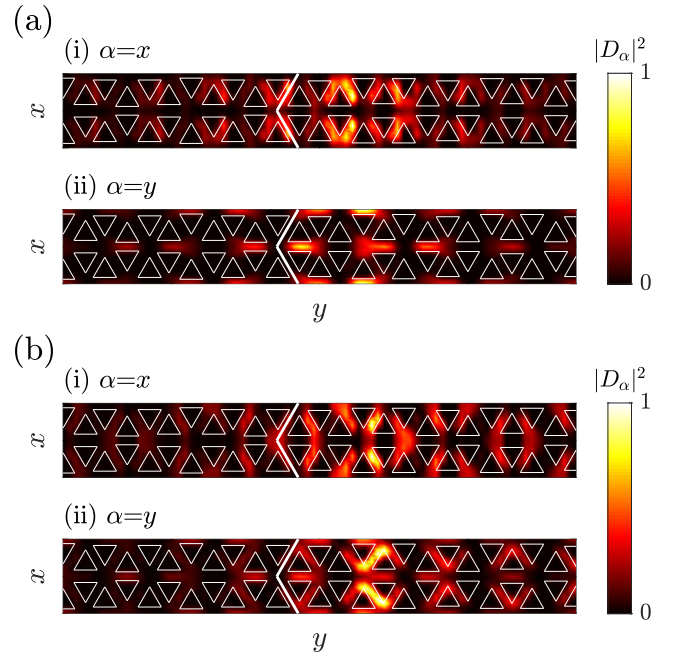


Figure 10. The x and y components of the electric displacement field profile of the guided modes for the armchair interface structure of triangular holes at $z = 0$. These modes are taken at the point of minimum loss, $k_x a = 0.017796$, for (a) the upper guided band labelled as State 1 in Fig. 8 and (b) the lower guided band labelled as State 2 in Fig. 8.

structures proposed by Anderson and Subramania⁴³ and Barik *et al.*^{44,51}. Photonic band diagrams were acquired for each structure, the propagation losses for their topological edge states were investigated, and electromagnetic field modes for the points of minimum loss were shown. Although these topological edge states are known to provide scatter-free light propagation, none of the structures

seemed to perform particularly well in terms of minimizing propagation loss. Taking previously reported minimum losses of 15 dB/cm and 5 dB/cm for the W1 waveguide as a comparison^{30,31}, the three topological structures we have studied show minimum losses on the order of 10^2 and 10^3 dB/cm. The electromagnetic fields of the guided modes remain mostly along the structures' interfaces, however these edge states are not shown to be tightly confined.

From the studied structures, the zigzag interface of circular holes provides the lowest minimum loss (and therefore the greatest loss length), however it is only marginally better than the armchair interface of circular holes. The armchair interface, on the other hand, is shown to be much more lossy than the other two structures and has much more difficulty in confining the edge state modes. Nonetheless, the armchair interface structure of triangular holes was the only structure to have its edge states fall below the light line.

If these topological structures are expected to be

worthwhile solutions to maximize the confinement of light, significant optimization methods to the structures' parameters or topologies must be applied. The guided-mode expansion is certainly an appropriate tool to do so, thanks to its ability to efficiently analyze complex photonic crystal slab structures.

While finishing this work, we recently became aware of alternative topological edge-state PC structures, including those by Shalaev *et al.*⁶⁰, and He *et al.*⁶¹, which may be more promising in terms of reducing intrinsic propagation losses. Future work will also examine these two structures.

ACKNOWLEDGMENTS

This work was supported by the Natural Sciences and Engineering Research Council of Canada, Queen's University and the Canadian Foundation for Innovation.

-
- * 14ers4@queensu.ca
 † juan.vasco@epfl.ch
 ‡ shughes@queensu.ca
- ¹ Kazuaki Sakoda, *Optical Properties of Photonic Crystals*, 2nd ed., Springer Series in Optical Sciences (Springer-Verlag, Berlin Heidelberg, 2005).
 - ² M. Patterson, S. Hughes, S. Schulz, D. M. Beggs, T. P. White, L. O'Faolain, and T. F. Krauss, "Disorder-induced incoherent scattering losses in photonic crystal waveguides: Bloch mode reshaping, multiple scattering, and breakdown of the Beer-Lambert law," *Physical Review B* **80**, 195305 (2009).
 - ³ Jakob Rosenkrantz de Lasson, *Modeling and Simulations of Light Emission and Propagation in Open Nanophotonic Systems*, Ph.D. thesis, Technical University of Denmark (DTU), Lyngby (2015).
 - ⁴ William Cartar, Jesper Mørk, and Stephen Hughes, "Self-consistent Maxwell-Bloch model of quantum-dot photonic-crystal-cavity lasers," *Physical Review A* **96**, 023859 (2017).
 - ⁵ Thomas F. Krauss, "Why do we need slow light?" *Nature Photonics* **2**, 448–450 (2008).
 - ⁶ M. Notomi, K. Yamada, A. Shinya, J. Takahashi, C. Takahashi, and I. Yokohama, "Extremely Large Group-Velocity Dispersion of Line-Defect Waveguides in Photonic Crystal Slabs," *Physical Review Letters* **87**, 253902 (2001).
 - ⁷ Gerasimos Angelatos, *Theory and Applications of Light-Matter Interactions in Quantum Dot Nanowire Photonic Crystal Systems*, Thesis (2015).
 - ⁸ Yurii A. Vlasov, Martin O'Boyle, Hendrik F. Hamann, and Sharee J. McNab, "Active control of slow light on a chip with photonic crystal waveguides," *Nature* **438**, 65–69 (2005).
 - ⁹ Toshihiko Baba, "Slow light in photonic crystals," *Nature Photonics* **2**, 465–473 (2008).
 - ¹⁰ Momchil Minkov and Vincenzo Savona, "Wide-band slow light in compact photonic crystal coupled-cavity waveguides," *Optica* **2**, 631–634 (2015).
 - ¹¹ Nobuyuki Matsuda, Takumi Kato, Ken-ichi Harada, Hiroki Takesue, Eiichi Kuramochi, Hideaki Taniyama, and Masaya Notomi, "Slow light enhanced optical nonlinearity in a silicon photonic crystal coupled-resonator optical waveguide," *Optics Express* **19**, 19861–19874 (2011).
 - ¹² Yao Zhang and Baojun Li, "Photonic crystal-based bending waveguides for optical interconnections," *Optics Express* **14**, 5723–5732 (2006).
 - ¹³ Yoshihiro Akahane, Takashi Asano, Bong-Shik Song, and Susumu Noda, "High-Q photonic nanocavity in a two-dimensional photonic crystal," *Nature* **425**, 944–947 (2003).
 - ¹⁴ Bong-Shik Song, Susumu Noda, Takashi Asano, and Yoshihiro Akahane, "Ultra-high-Q photonic double-heterostructure nanocavity," *Nature Materials* **4**, 207–210 (2005).
 - ¹⁵ Momchil Minkov, Vincenzo Savona, and Dario Gerace, "Photonic crystal slab cavity simultaneously optimized for ultra-high Q/V and vertical radiation coupling," *Applied Physics Letters* **111**, 131104 (2017).
 - ¹⁶ Takashi Asano, Yoshiaki Ochi, Yasushi Takahashi, Katsuhiko Kishimoto, and Susumu Noda, "Photonic crystal nanocavity with a Q factor exceeding eleven million," *Optics Express* **25**, 1769–1777 (2017).
 - ¹⁷ K. Hennessy, A. Badolato, M. Winger, D. Gerace, M. Atatüre, S. Gulde, S. Fält, E. L. Hu, and A. Imamoglu, "Quantum nature of a strongly coupled single quantum dot-cavity system," *Nature* **445**, 896–899 (2007).
 - ¹⁸ T. Yoshie, A. Scherer, J. Hendrickson, G. Khitrova, H. M. Gibbs, G. Rupper, C. Ell, O. B. Shchekin, and D. G. Deppe, "Vacuum Rabi splitting with a single quantum dot in a photonic crystal nanocavity," *Nature* **432**, 200–203 (2004).
 - ¹⁹ Bryan Ellis, Marie A. Mayer, Gary Shambat, Tomas Sarmiento, James Harris, Eugene E. Haller, and Jelena Vučković, "Ultralow-threshold electrically pumped quantum-dot photonic-crystal nanocavity

- laser,” *Nature Photonics* **5**, 297–300 (2011).
- 20 Kengo Nozaki, Takasumi Tanabe, Akihiko Shinya, Shinji Matsuo, Tomonari Sato, Hideaki Taniyama, and Masaya Notomi, “Sub-femtojoule all-optical switching using a photonic-crystal nanocavity,” *Nature Photonics* **4**, 477–483 (2010).
 - 21 Ulagalandha Perumal Dharanipathy, Momchil Minkov, Mario Tonin, Vincenzo Savona, and Romuald Houdré, “High-Q silicon photonic crystal cavity for enhanced optical nonlinearities,” *Applied Physics Letters* **105**, 101101 (2014).
 - 22 M. Notomi, E. Kuramochi, and H. Taniyama, “Ultra-high-Q Nanocavity with 1D Photonic Gap,” *Optics Express* **16**, 11095–11102 (2008).
 - 23 Yoshinori Tanaka, Takashi Asano, and Susumu Noda, “Design of Photonic Crystal Nanocavity With Q-Factor of $\sim 10^9$,” *Journal of Lightwave Technology* **26**, 1532–1539 (2008).
 - 24 J. P. Vasco, H. Vinck-Posada, P. T. Valentim, and P. S. S. Guimarães, “Modeling of Fano resonances in the reflectivity of photonic crystal cavities with finite spot size excitation,” *Optics Express* **21**, 31336–31346 (2013).
 - 25 Keisuke Kitano, Katsuyoshi Suzuki, Kenji Ishizaki, and Susumu Noda, “Three-dimensional photonic crystals fabricated by simultaneous multidirectional etching,” *Physical Review B* **91**, 155308 (2015).
 - 26 Timothy Y. M. Chan, Ovidiu Toader, and Sajeev John, “Photonic band-gap formation by optical-phase-mask lithography,” *Physical Review E* **73**, 046610 (2006).
 - 27 J. D. Joannopoulos, ed., *Photonic Crystals: Molding the Flow of Light*, 2nd ed. (Princeton University Press, Princeton, 2008).
 - 28 Lucio Claudio Andreani and Dario Gerace, “Photonic-crystal slabs with a triangular lattice of triangular holes investigated using a guided-mode expansion method,” *Physical Review B* **73**, 235114 (2006).
 - 29 M. Patterson, S. Hughes, S. Combrié, N.-V.-Quynh Tran, A. De Rossi, R. Gabet, and Y. Jaouën, “Disorder-Induced Coherent Scattering in Slow-Light Photonic Crystal Waveguides,” *Physical Review Letters* **102**, 253903 (2009).
 - 30 E. Kuramochi, M. Notomi, S. Hughes, A. Shinya, T. Watanabe, and L. Ramunno, “Disorder-induced scattering loss of line-defect waveguides in photonic crystal slabs,” *Phys. Rev. B* **72**, 161318(R) (2005).
 - 31 Liam O’Faolain, Thomas P. White, David O’Brien, Xiaodong Yuan, Michael D. Settle, and Thomas F. Krauss, “Dependence of extrinsic loss on group velocity in photonic crystal waveguides,” *Opt. Express* **15**, 13129–13138 (2007).
 - 32 Juntao Li, Thomas P. White, Liam O’Faolain, Alvaro Gomez-Iglesias, and Thomas F. Krauss, “Systematic design of flat band slow light in photonic crystal waveguides,” *Opt. Express* **16**, 6227–6232 (2008).
 - 33 Nishan Mann, Sylvian Combrié, Pierre Colman, Mark Patterson, Alfredo De Rossi, and Stephen Hughes, “Reducing disorder-induced losses for slow light photonic crystal waveguides through Bloch mode engineering,” *Optics Letters* **38**, 4244–4247 (2013).
 - 34 Nishan Mann, Mark Patterson, and Stephen Hughes, “Role of Bloch mode reshaping and disorder correlation length on scattering losses in slow-light photonic crystal waveguides,” *Physical Review B* **91**, 245151 (2015).
 - 35 S. Hughes, L. Ramunno, Jeff F. Young, and J. E. Sipe, “Extrinsic Optical Scattering Loss in Photonic Crystal Waveguides: Role of Fabrication Disorder and Photon Group Velocity,” *Physical Review Letters* **94**, 033903 (2005).
 - 36 Dario Gerace and Lucio Claudio Andreani, “Effects of disorder on propagation losses and cavity q-factors in photonic crystal slabs,” *Photonics and Nanostructures - Fundamentals and Applications* **3**, 120 (2005).
 - 37 N. Le Thomas and R. Houdré, “Group velocity and energy transport velocity near the band edge of a disordered coupled cavity waveguide: An analytical approach,” *J. Opt. Soc. Am. B* **27**, 2095–2101 (2010).
 - 38 Mohamed Sabry Mohamed, Yiming Lai, Momchil Minkov, Vincenzo Savona, Antonio Badolato, and Romuald Houdré, “Influence of Disorder and Finite-Size Effects on Slow Light Transport in Extended Photonic Crystal Coupled-Cavity Waveguides,” *ACS Photonics* **5**, 4846–4853 (2018).
 - 39 Dario Gerace and Lucio Claudio Andreani, “Disorder-induced losses in photonic crystal waveguides with line defects,” *Optics Letters* **29**, 1897–1899 (2004).
 - 40 Weiwei Song, Ryan A. Integlia, and Wei Jiang, “Slow light loss due to roughness in photonic crystal waveguides: An analytic approach,” *Physical Review B* **82**, 235306 (2010).
 - 41 Momchil Minkov and Vincenzo Savona, “Effect of hole-shape irregularities on photonic crystal waveguides,” *Optics Letters* **37**, 3108–3110 (2012).
 - 42 J. P. Vasco and S. Hughes, “Exploiting Long-Range Disorder in Slow-Light Photonic Crystal Waveguides: Anderson Localization and Ultra-high Q/V Cavities,” *ACS Photonics* **6**, 2926–2932 (2019).
 - 43 P. Duke Anderson and Ganapathi Subramania, “Unidirectional edge states in topological honeycomb-lattice membrane photonic crystals,” *Optics Express* **25**, 23293–23301 (2017).
 - 44 Sabyasachi Barik, Hirokazu Miyake, Wade DeGottardi, Edo Waks, and Mohammad Hafezi, “Two-dimensionally confined topological edge states in photonic crystals,” *New Journal of Physics* **18**, 113013 (2016).
 - 45 Nikhil Parappurath, Filippo Alpegiani, L. Kuipers, and Ewold Verhagen, “Direct Observation of Topological Edge States in Silicon Photonic Crystals: Spin, Dispersion, and Chiral Routing,” [arXiv:1811.10739](https://arxiv.org/abs/1811.10739) (2018).
 - 46 Ling Lu, John D. Joannopoulos, and Marin Soljačić, “Topological photonics,” *Nature Photonics* **8**, 821–829 (2014).
 - 47 Ling Lu, Chen Fang, Liang Fu, Steven G. Johnson, John D. Joannopoulos, and Marin Soljai, “Symmetry-protected topological photonic crystal in three dimensions,” *Nature Physics* **12**, 337–340 (2016).
 - 48 Long-Hua Wu and Xiao Hu, “Scheme for Achieving a Topological Photonic Crystal by Using Dielectric Material,” *Physical Review Letters* **114**, 223901 (2015).
 - 49 Mahmoud Jalali Mehrabad, Andrew P. Foster, René Dost, A. Mark Fox, Maurice S. Skolnick, and Luke R. Wilson, “Chiral topological photonics with an embedded quantum emitter,” [arXiv:1912.09943](https://arxiv.org/abs/1912.09943) (2019).
 - 50 María Blanco de Paz, Chiara Devescovi, Geza Giedke, Juan José Saenz, Maia G. Vergniory, Barry Bradlyn, Dario Bercioux, and Aitzol García-Etxarri, “Tutorial: Computing Topological Invariants in 2D Photonic Crystals,” *Advanced Quantum Technologies* **3**, 1900117 (2020).

- ⁵¹ Sabyasachi Barik, Aziz Karasahin, Christopher Flower, Tao Cai, Hirokazu Miyake, Wade DeGottardi, Mohammad Hafezi, and Edo Waks, “A topological quantum optics interface,” *Science* **359**, 666–668 (2018).
- ⁵² Allen Taflove and Susan C. Hagness, *Computational Electrodynamics: The Finite-Difference Time-Domain Method* (Artech House, 2005).
- ⁵³ Hwi Kim, Junghyun Park, and Byoung-ho Lee, *Fourier Modal Method and Its Applications in Computational Nanophotonics* (CRC Press, 2012).
- ⁵⁴ Steven G. Johnson and J. D. Joannopoulos, “Block-iterative frequency-domain methods for Maxwell’s equations in a planewave basis,” *Optics Express* **8**, 173–190 (2001).
- ⁵⁵ Mark Patterson, *Classical and Quantum Optical Properties of Slow Light Photonic Crystal Waveguides*, Thesis (2009).
- ⁵⁶ Yan Zhao, Pavel Belov, and Yang Hao, “Accurate modeling of the optical properties of left-handed media using a finite-difference time-domain method,” *Physical Review E* **75**, 037602 (2007).
- ⁵⁷ Jonathan Andreasen, Hui Cao, Allen Taflove, Prem Kumar, and Chang-qi Cao, “Finite-difference time-domain simulation of thermal noise in open cavities,” *Physical Review A* **77**, 023810 (2008).
- ⁵⁸ N. N. Potravkin, I. A. Perezhogin, and V. A. Makarov, “Numerical solution of Maxwell equations by a finite-difference time-domain method in a medium with frequency and spatial dispersion,” *Physical Review E* **86**, 056706 (2012).
- ⁵⁹ Will Cartar, *Theory and Modelling of Light-Matter Interactions in Photonic Crystal Cavity Systems Coupled to Quantum Dot Ensembles*, Thesis (2017).
- ⁶⁰ Mikhail I. Shalaev, Wiktor Walasik, Alexander Tsukernik, Yun Xu, and Natalia M. Litchinitser, “Robust topologically protected transport in photonic crystals at telecommunication wavelengths,” *Nature Nanotechnology* **14**, 31–34 (2019).
- ⁶¹ Xin-Tao He, En-Tao Liang, Jia-Jun Yuan, Hao-Yang Qiu, Xiao-Dong Chen, Fu-Li Zhao, and Jian-Wen Dong, “A silicon-on-insulator slab for topological valley transport,” *Nature Communications* **10**, 1–9 (2019).